Thermochimica Acta, 219 (1993) 269–282
Elsevier Science Publishers B.V., Amsterdam

Studies on the formation of γ-Fe_2O_3 by thermal decomposition of ferrous malate dihydrate

A.K. Nikumbh *, A.A. Latkar and M.M. Phadke
Department of Chemistry, University of Poona, Ganeshkhind, Pune 411 007 (India)

(Received 20 August 1992)

Abstract

Ferrous malate dihydrate ($FeC_4H_4O_5 \cdot 2H_2O$) was prepared and its thermal decomposition studied by means of simultaneous thermal analysis (TGA, DTA, DTG) curves supplemented with two-probe d.c. electrical conductivity measurements under the atmospheres of static air, dynamic nitrogen and dynamic air. Dynamic air containing water vapour was found to be the most suitable atmosphere for the synthesis of γ-Fe_2O_3. The isothermal decomposition of $FeC_4H_4O_5 \cdot 2H_2O$ for various intermediate phases occurring at different ranges of temperature under the above atmospheres was studied using IR spectral studies, C and H analyses and X-ray diffraction data. This study reveals the formation of the anhydrous carboxylate ($FeC_4H_4O_5$), which then oxidatively decomposes to α-Fe_2O_3, with probable intermediates FeO and Fe_3O_4, along with some $FeC_4H_4O_5$ and γ-Fe_2O_3. Both polar and non-polar gases were obtained during the decomposition of $FeC_4H_4O_5 \cdot 2H_2O$ under nitrogen atmosphere; these were analysed using gas–liquid chromatography. The γ-Fe_2O_3 synthesized was characterized by X-ray diffraction, magnetic hysteresis, scanning electron microscopy and Mössbauer spectroscopy.

INTRODUCTION

The important application of γ-Fe_2O_3 (meghemite) in magnetic recording tapes and ferrite components is well known. Gamma ferric oxide (γ-Fe_2O_3) is a ferrimagnetic compound with the inverse spinel structures, in which iron(III) cations occupy both the tetrahedral (A) and octahedral (B) sites; it is usually assumed to have a colinear magnetic structure consisting of two sublattices.

γ-Fe_2O_3 is obtained commercially from synthetic goethite (α-FeO(OH)) involving dehydration to α-Fe_2O_3, reduction to Fe_3O_4 and final, reoxidation to γ-Fe_2O_3 [1]. There are reports on the preparation of γ-Fe_2O_3 from iron(II) carboxylate by using iron(II) oxalate dihydrate [2–5]. Another method for the synthesis of γ-Fe_2O_3 from thermal decomposition of ferrous oxalate dihydrate using d.c. electrical conductivity for characterization has

* Corresponding author.

been reported [6, 7]. Recently the syntheses of γ-Fe_2O_3 by the thermal decomposition of ferrous fumarate [8], ferrous succinate [9], ferrous tartarate [10] and ferrous malonate [11] have been reported. However, the formation of γ-Fe_2O_3 during the decomposition of $FeC_4H_4O_5 \cdot 2H_2O$ (ferrous malate dihydrate) has not been investigated yet. In the present work, the thermal decomposition of ferrous malate dihydrate has been studied using two-probe d.c. electrical conductivity to investigate the conditions for the preparation of γ-Fe_2O_3. This study has been supplemented with TGA, DTG and DTA, X-ray diffraction, IR spectroscopy and gas–liquid chromatography.

EXPERIMENTAL

Preparation of $FeC_4H_4O_5 \cdot 2H_2O$

Ferrous malate dihydrate was prepared according to the similar procedure described in ref. 12. $FeCl_2$ (15 g) was placed in a three-necked flask under a stream of dry nitrogen. Oxygen-free distilled water (100 ml) was then added, and the solution was stirred vigorously with a magnetic stirrer. Sodium malate (8 g) was dissolved in distilled water, and the solution was added slowly with stirring to the solution of $FeCl_2$. Distilled acetone (250 ml) was then added, and after some time ferrous malate dihydrate ($FeC_4H_4O_5 \cdot 2H_2O$) separated out as a fine crystalline precipitate. This was filtered, washed with cold acetone and dried in vacuo.

Elemental analysis was made for $FeC_4H_4O_5 \cdot 2H_2O$ (wt.%): C, found 21.5, calc. 21.4; H, found 3.60, calc. 3.57; Fe, found 25.04, calc. 24.95. The IR spectra showed frequencies corresponding to the carboxylate group, hydroxyl group, metal–oxygen, etc. The bidentate linkage of the carboxylate group with the metal was confirmed on the basis of the difference between the antisymmetric and symmetric stretching frequencies. The presence of two molecules of water of crystallisation was confirmed on the basis of the thermal analysis curves. The compound $FeC_4H_4O_5 \cdot 2H_2O$ has a magnetic moment of 5.04 BM, which indicates that the compound has free spin with sp^3d^2 hybridisation.

The thermal analysis curves were obtained with a Netzsch instrument in an atmosphere of dynamic dry nitrogen, dynamic dry air (flowing at the rate of 90 ml min^{-1}) and static air in the temperature range of ambient to 700°C with a heating rate of 10°C min^{-1}. The two-probe d.c. electrical conductivity (apparatus fabricated in the department) was measured on a Philips microvoltmeter PP 9004 instrument under static air, dynamic dry air, dynamic dry nitrogen and dynamic air containing water vapour [6]. The heating rate was adjusted to 10°C min^{-1} and flow rate for different atmospheres was maintained at 90 ml min^{-1}. The evolution of various gases

during the thermal decomposition was recorded on Shimadzu Ria and Hewlett–Packard instruments using nitrogen as the carrier gas. IR spectra were recorded on a Perkin–Elmer Model 783 spectrophotometer using nujol mull. The powder X-ray diffraction results were obtained on a PW 1730 Philips X-ray diffractometer using Cu Kα radiation (λ = 1.5405 Å; nickel filter).

The morphology of γ-Fe_2O_3 particles was investigated using a Cambridge steroscan 150 instrument. The magnetic properties were studied using an alternating electromagnet type hysteresis loop tracer [13]. The Mössbauer spectra were obtained with a constant acceleration spectrometer coupled with a multichannel analyser assembled in the University Department of Physics.

RESULTS AND DISCUSSION

Static air atmosphere

The dehydration step of $FeC_4H_4O_5 \cdot 2H_2O$ in Fig. 1(a) could be detected by the presence of a broad endothermic peak in the DTA curves at 140°C and also a broad peak at the same temperature on the DTG curve. However, the TGA curve showed continuous weight loss around 60–180°C,

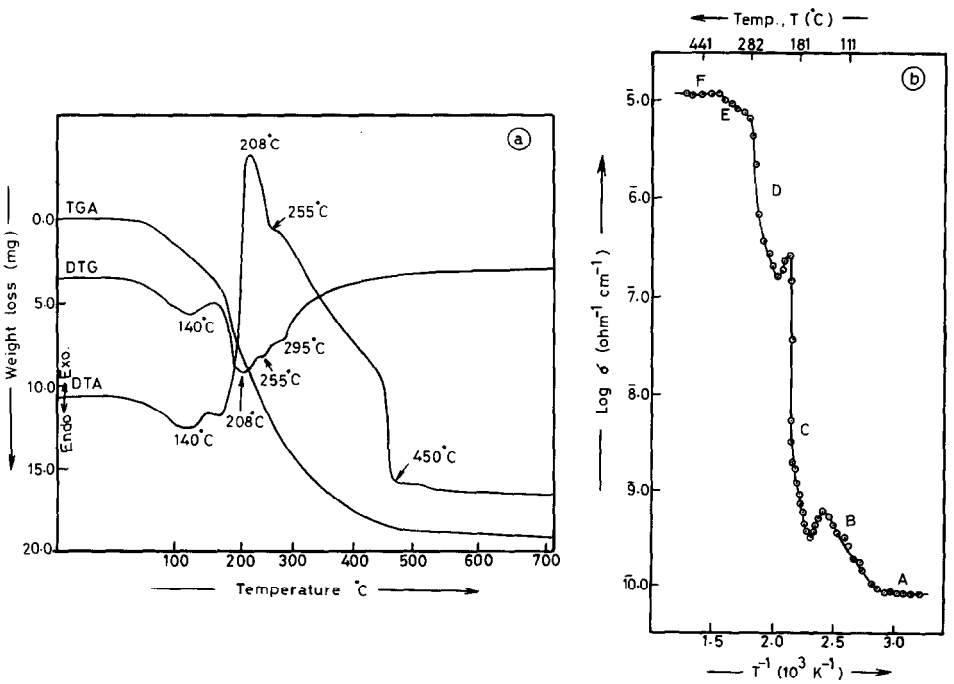

Fig. 1. Static air atmosphere: (a), TGA, DTA and DTG curves for $FeC_4H_4O_5 \cdot 2H_2O$; (b), plot of log σ vs. T^{-1} for $FeC_4H_4O_5 \cdot 2H_2O$ (⊙, during decomposition).

TABLE 1

X-Ray diffraction data for $FeC_4H_4O_5 \cdot 2H_2O$ [a]

Observed *d*-spacing values (present study) (Å)	Observed *d*-spacing values (present study) (Å)
4.00 (60)	1.97 (50)
3.54 (63)	1.62 (23)
3.38 (5)	1.57 (13)
2.80 (100)	1.50 (12)
2.32 (31)	1.42 (12)
2.29 (25)	1.14 (9)
2.01 (42)	

[a] The values given in parentheses are intensities relative to the linewidth intensity of 100.

indicating that the anhydrous malate ($FeC_4H_4O_5$) formed at this temperature is unstable. The plot of $\log \sigma$ vs. T^{-1} in Fig. 1(b) showed that σ was initially constant (Region A). IR spectral and X-ray diffraction data (Table 1) indicated no observable change in the isothermally heated sample of $FeC_4H_4O_5 \cdot 2H_2O$ for this region. The value of σ then increased from 75 to 143°C and a decrease up to 175°C (Region B) for the dehydration step. The isothermally heated $FeC_4H_4O_5 \cdot 2H_2O$ sample under this atmosphere at 150°C did not have H–OH bands in the IR spectrum. Elemental analysis agreed well with the anhydrous compound $FeC_4H_4O_5$, and the X-ray diffraction pattern indicated that the sample was less crystalline than the parent compound $FeC_4H_4O_5 \cdot 2H_2O$ (Table 2). Region B was therefore said to correspond to the dehydration of $FeC_4H_4O_5 \cdot 2H_2O$.

TABLE 2

X-Ray diffraction data for anhydrous $FeC_4H_4O_5$ obtained from $FeC_4H_4O_5 \cdot 2H_2O$ by heating in an atmosphere of static air at 150°C [a]

Observed *d*-spacing for $FeC_4H_4O_5$ (Å)	Observed *d*-spacing for $FeC_4H_4O_5$ (Å)
4.02 (43)	2.26 (21)
3.86 (16)	2.12 (18)
3.52 (60)	1.93 (35)
3.30 (21)	1.77 (20)
2.87 (28)	1.68 (31)
2.81 (100)	1.63 (16)
2.52 (25)	1.57 (10)
2.34 (30)	

[a] The values given in parentheses are intensities relative to the linewidth intensity 100.

The DTA curve in Fig. 1(a) had a very strong and broad exothermic peak at 208°C (and a hump at 255°C); a broad peak at the same temperature along with a hump at 255°C was observed on the DTG curve, corresponding to the oxidative decomposition of $FeC_4H_4O_5$. Owing to the broadness of this peak, the various intermediates formed during this step could not be detected; further, the TGA curve exhibited continuous weight loss until crystallisation to α-Fe_2O_3 occurred.

The plot of $\log \sigma$ vs. T^{-1} for $FeC_4H_4O_5$ shown in Fig. 1(b) had various values of conductivities, corresponding to the various intermediates formed during the oxidative decomposition of $FeC_4H_4O_5$.

The value of σ steadily increased from 175 to 220°C (Region C), and the IR spectrum of the isothermally heated $FeC_4H_4O_5 \cdot 2H_2O$ sample at 210°C showed a decrease in intensity of coordinated carboxylates bands; in addition, bands at 395 cm^{-1} (s) and 350 cm^{-1} (m) occurred for metal–oxygen stretching frequencies due to the presence of iron oxide [14]. The X-ray powder diffraction pattern of this isothermally heated sample showed the structure to be polycrystalline in nature; the peaks corresponding to both $FeC_4H_4O_5$ and FeO were observed.

Although a tendency for a steep increase in σ was observed at 225°C (Region D), the characteristic high value of Fe_3O_4 ($\approx 10^{-3}$ ohm^{-1} cm^{-1}) could be obtained under dynamic conditions. A decrease in σ was seen at 300°C (Region E), probably due to the formation of semiconducting γ-Fe_2O_3. The sample in Region E (290–350°C) is mainly γ-Fe_2O_3 with traces of Fe_3O_4; the X-ray powder diffraction pattern was generally broad, having peaks corresponding mainly to γ-Fe_2O_3 and traces of Fe_3O_4. The IR spectrum of $FeC_4H_4O_5 \cdot 2H_2O$ heated at 300°C showed no bands due to a coordinated carboxylate group. However, strong broad bands corresponding to Fe–O stretching frequencies were observed. This part of the graph is followed by Region F (i.e. above 400°C), corresponding to the complete transformation of γ-Fe_2O_3 to α-Fe_2O_3.

When the reaction is carried out using the static atmosphere, the gaseous products act as a gas buffer for the solid state reaction and some reaction is ill defined. For example, the role of the two water molecules in $FeC_4H_4O_5 \cdot 2H_2O$ and the role of atmospheric oxygen in the solid-state reaction carried out in static air can be clarified by comparing the data for different physical properties for the same reaction carried out in a dynamic dry nitrogen atmosphere.

Dynamic nitrogen atmosphere

The TGA curve for $FeC_4H_4O_5 \cdot 2H_2O$ in Fig. 2(a) showed a clear dehydration step corresponding to the loss of the two water molecules from 30 to 195°C, and this stage is supported by the presence of an endothermic peak at 137°C on the DTA curve and a peak at 140°C on the DTG curve.

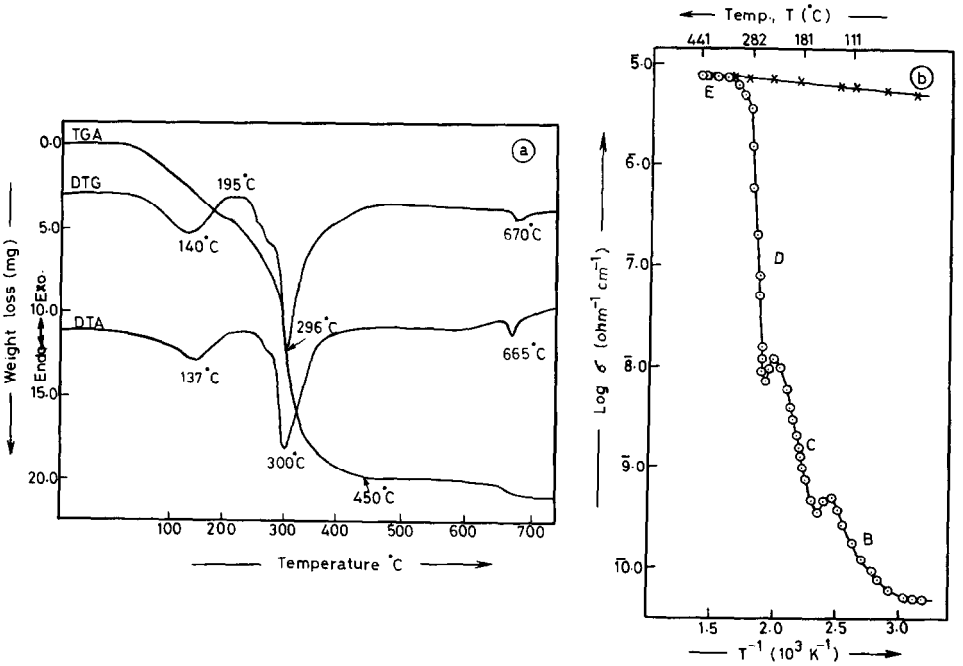

Fig. 2. Dynamic nitrogen atmosphere: (a), TGA, DTA and DTG curves for $FeC_4H_4O_5 \cdot 2H_2O$; (b), plot of log σ vis. T^{-1} for $FeC_4H_4O_5 \cdot 2H_2O$ (⊙, during decomposition; ×, cooling cycle).

The plot of log σ vs. T^{-1} in Fig. 2(b) showed a clear peak at 143°C (Region B) corresponding to the dehydration step; the $FeC_4H_4O_5 \cdot 2H_2O$ sample heated isothermally under dynamic dry nitrogen at 140°C showed no H–OH bands in the IR spectrum. Elemental analysis agreed well with the anhydrous compound $FeC_4H_4O_5$ and the X-ray diffraction pattern showed a decrease in interplanar spacing, which was similar to that obtained for the anhydrous carboxylate ($FeC_4H_4O_5$) under a static air atmosphere given in Table 2. Region B, therefore, corresponded to the dehydration of $FeC_4H_4O_5 \cdot 2H_2O$.

The decomposition steps could be seen on the DTA curve at 300°C (296°C on the DTG curve) and crystallisation to the α-Fe_2O_3 phase was observed at 665°C on the DTA curve and 670°C on the DTG curve. The TGA curve showed weight loss from 195 to 450°C and a further weight loss from 450 to 690°C. However, the weight loss calculated from the TGA curve could not reveal the formation of any particular single intermediate species. The plot of log σ vs. T^{-1} clearly showed the different intermediate phases which occurred during decomposition. Here, the cooling curve was also noted to test the purity of Fe_3O_4 formed. The sample obtained on isothermally heating $FeC_4H_4O_5 \cdot 2H_2O$ in Region C (150–240°C) showed that the IR bands corresponding to Fe–O stretching frequencies increased,

TABLE 3

X-Ray diffraction data for $FeC_4H_4O_5$ and FeO obtained from $FeC_4H_4O_5 \cdot 2H_2O$ by heating in an atmosphere of nitrogen at 240°C [a]

Observed d-spacing values (present study) (Å)	FeO (cubic) d-spacing values [b] (Å)
4.10 (15)	
3.54 (17)	
3.32 (13)	
2.93 (20)	
2.83 (62)	
2.51 (100)	2.490 (80)
2.41 (24)	
2.33 (9)	
2.24 (13)	
2.15 (71)	2.153 (100)
2.00 (39)	
1.86 (28)	
1.71 (28)	
1.64 (20)	
1.52 (40)	1.523 (60)
1.31 (10)	1.299 (25)
1.08 (15)	1.077 (15)

[a] The values given in parentheses are intensities relative to the linewidth intensity of 100.
[b] Ref. 15.

and those due to coordinated carboxylate bands decreased in intensty. The X-ray diffraction pattern showed sharp lines, indicating that the sample is predominantly crystalline. The pattern fits with the data for cubic FeO [15] and some $FeC_4H_4O_5$ (Table 3).

A steep increase in σ was observed within the temperature range 250–310°C (in Region D) (Fig. 2(b)). A sample obtained by isothermal heating in dry nitrogen at 290°C was probably a mixture of FeO and Fe_3O_4. The X-ray diffraction pattern was generally broad, and comparable with data reported for FeO [15] and Fe_3O_4 [16].

X-Ray diffraction pattern data for a sample from the dry nitrogen atmosphere run obtained at 440°C (Region E) showed sharp lines and were comparable with the data reported [16] for Fe_3O_4 (Table 4). The sample thus obtained at 440°C showed a negligible variation in σ with variation of temperature. This behaviour is characteristic of Fe_3O_4 [17–19].

Comparison of the solid-state thermal decomposition reactions of $FeC_4H_4O_5 \cdot 2H_2O$ in static air and in dynamic dry nitrogen showed the following main differences.

(1) The temperatures corresponding to dehydration and decomposition from DTA and DTG curves recorded under nitrogen atmosphere were

TABLE 4

X-Ray diffraction data for Fe_3O_4 obtained from $FeC_4H_4O_5 \cdot 2H_2O$ by heating in an atmosphere of nitrogen at 440°C [a]

Observed *d*-spacing values (present study) (Å)	Fe_3O_4 *d*-spacing values [b] (Å)
	4.85 (8)
2.95 (27)	2.967 (30)
2.51 (100)	2.532 (100)
2.44 (11)	2.424 (8)
2.06 (15)	2.099 (20)
1.71 (14)	1.715 (10)
1.65 (23)	1.616 (30)
1.49 (36)	1.485 (40)
	1.419 (2)
	1.328 (4)
1.27 (8)	1.281 (10)
	1.266 (4)
	1.212 (2)
1.12 (5)	1.212 (4)
1.09 (10)	1.093 (12)
	1.050 (6)

[a] The values given in parentheses are intensities relative to the linewidth intensity of 100.
[b] Ref. 16.

resolvable and matches with the changes observed in plots of log σ vs. T^{-1}, whereas the curves obtained under static air were quite complex.

(2) Malate was intimately associated with the decomposition product up to 260°C in static air and a dry nitrogen atmosphere.

(3) Region E, corresponding to the γ-Fe_2O_3 formation stage, could not be identified under nitrogen, whereas the region could be detected under static air.

The nature of the solid-state decomposition of $FeC_4H_4O_5 \cdot 2H_2O$ is influenced by the composition of the atmosphere, so it was considered advantageous to undertake similar measurements in other controlled atmosphere.

Dynamic air atmosphere

The dehydration step was shown by an endothermic peak on the DTA curve at 135°C and a peak at the same temperature on a DTG curve. The TGA curve showed a weigh loss from room temperature to 160°C, corresponding to the loss of two water molecules (Fig. 3(a)); a Region B was observed for this step in the plot of log σ vs. T^{-1} (see Fig. 3(b)). The broad exothermic peak corresponding to oxidative decomposition was found on

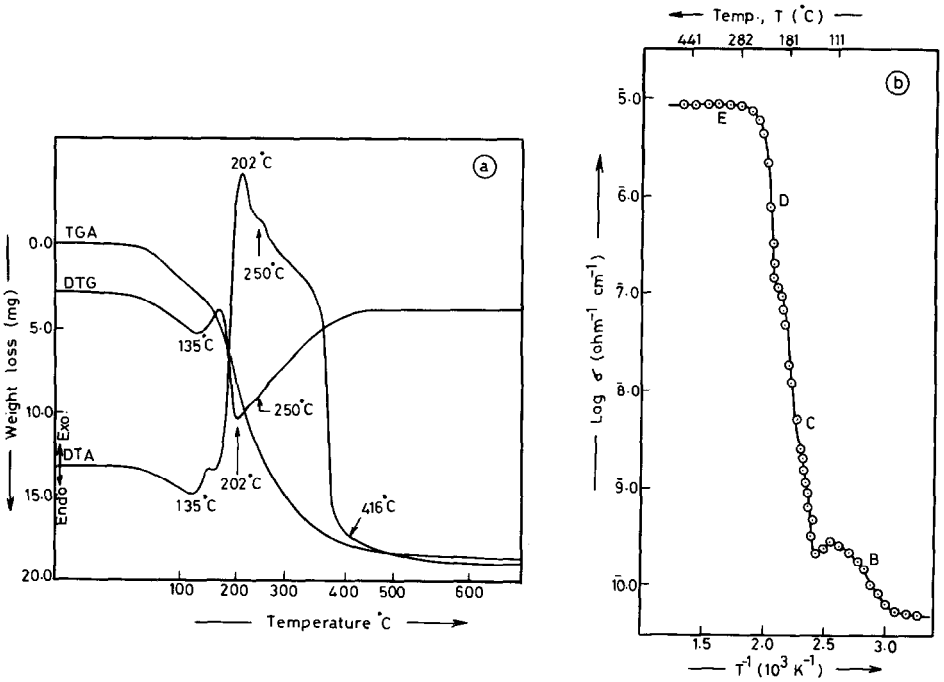

Fig. 3. Dynamic air atmosphere: (a), TGA, DTA and DTG curves for $FeC_4H_4O_5 \cdot 2H_2O$; (b), plot of log σ vs. T^{-1} for $FeC_4H_4O_5 \cdot 2H_2O$ (⊙, during decomposition).

the DTA curve at 202°C (hump at 250°C), a peak at this temperature was also seen on the DTG curve and the TGA curve showed a continuous weight loss in this region. In general, the thermal analysis (TGA, DTA and DTG) curves obtained were similar to Fig. 1(a). The plot of log σ vs. T^{-1} in Fig. 3(b) showed that the decomposition is similar to that shown in Fig. 1(b). The isothermal decomposition under a dynamic air atmosphere for $FeC_4H_4O_5 \cdot 2H_2O$ in various temperature ranges (Regions C–E) showed that the products obtained were similar to those from isothermally decomposing $FeC_4H_5O_5 \cdot 2H_2O$ under a static air atmosphere. The only difference found when using this atmosphere was that there was no formation of γ-Fe_2O_3.

These observations suggest that the solid state decomposition of $FeC_4H_4O_5 \cdot 2H_2O$ under the buffer atmosphere in static air and in dynamic air follow slightly different patterns. Experimental data determined in dynamic air containing water vapour could provide further information on the solid state thermal decomposition of $FeC_4H_4O_5 \cdot 2H_2O$.

Dynamic air containing water vapour

The progress of the decomposition of $FeC_4H_4O_5 \cdot 2H_2O$ in dynamic air containing water vapour (Fig. 4(a)), as studied by IR spectra, elemental

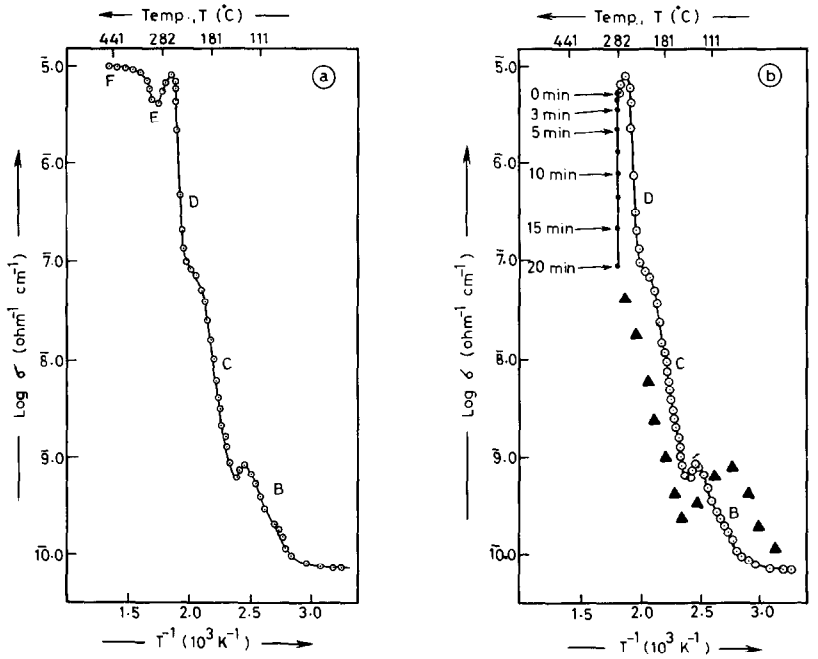

Fig. 4. (a) Plot of log σ vs. T^{-1} for $FeC_4H_4O_5 \cdot 2H_2O$ during decomposition in dynamic air containing water vapour. (b) Plot of log σ vs. T^{-1} for $FeC_4H_4O_5 \cdot 2H_2O$ during decomposition in dynamic air containing water vapour: ⊙, during decomposition; ▲, cooling cycle for γ-Fe_2O_3.

analyses and X-ray diffraction, indicated the formation of $FeC_4H_4O_5$ at 140°C. There was a steep increase in the value of σ between 140 and 200°C (Region C), indicating the presence of a mixture of FeO and some $FeC_4H_4O_5$. This increase in σ was followed by a very steep increase from 205 to 280°C before the sample underwent irreversible transformation into α-Fe_2O_3 at 400°C. A well resolved kink was observed at 300°C. Region D from 205 to 280°C indicated the formation of Fe_3O_4. The IR spectral study and X-ray diffraction pattern revealed that $FeC_4H_4O_5$ was stable up to 250°C, along with Fe_3O_4, and from 250 to 290°C only monophasic Fe_3O_4 was present. The well resolved kink at 300°C is characteristic of the formation of γ-Fe_2O_3 [6] and above 395°C complete irreversible transformation of α-Fe_2O_3 occurred.

A careful analysis of the time-dependent σ measurements in the temperature range 290–300°C revealed the following points.

(a) There was no variation in the σ value with time up to 300°C.

(b) At 300°C the σ value changed from 6.60 to 8.92 Ω^{-1} cm^{-1} within 20 min (Fig. 4(b)).

(c) There was no further decrease of σ above 300°C.

(d) For the sample heated to 300°C and then cooled, the log σ vs. T^{-1} curves for cooling and heating did not overlap (Fig. 4(b)).

TABLE 5

X-Ray diffraction data of γ-Fe_2O_3 obtained from $FeC_4H_4O_5 \cdot 2H_2O$ by heating under dynamic air containing water vapour at 300°C [a]

Observed d-spacing values for γ-Fe_2O_3 (present study) (Å)	γ-Fe_2O_3 (tetragonal) d-spacing values [b] (Å)
5.89 (8)	6.94 (2)
	5.90 (6)
4.80 (10)	5.33 (1)
	4.82 (6)
3.71 (8)	4.29 (2)
3.41 (5)	3.73 (6)
	3.40 (7)
2.96 (27)	3.20 (3)
2.77 (14)	2.95 (30)
2.63 (7)	2.78 (13)
2.51 (100)	2.638 (4)
	2.514 (100)
2.33 (5)	2.408 (2)
	2.315 (2)
2.09 (20)	2.23 (2)
	2.086 (15)
1.82 (5)	1.865 (1)
1.71 (25)	1.82 (3)
	1.701 (19)
1.61 (35)	1.67 (2)
	1.604 (20)
	1.55 (2)
1.48 (38)	1.523 (3)
	1.474 (40)
1.28 (12)	1.318 (6)
	1.272 (8)

[a] The values given in parentheses are intensities relative to the linewidth intensity of 100.
[b] Ref. 20.

The sample thus obtained was heated under nitrogen at 280°C to remove any water. The X-ray diffraction pattern of this sample (Table 5) was very sharp, indicating that the sample was highly crystalline, similar to the results reported for γ-Fe_2O_3 [20].

The magnetic hysteresis measurements made on this γ-Fe_2O_3 show that it has a coercive force H_c of 250.0 Oe, saturation magnetisation M_s of 73.5 emu g^{-1} and a ratio of remanence to saturation magnetisation M_R/M_S of 0.63. These values are comparable with the data given in ref. 4.

The Mössbauer spectrum showed six well-resolved narrow bands in the intensity ratio 3:2:1:1:2:3, and the value of the hyperfine field was found to be 495.5 ± 5.0 Koe, similar to that reported in ref. 21. Scanning electron

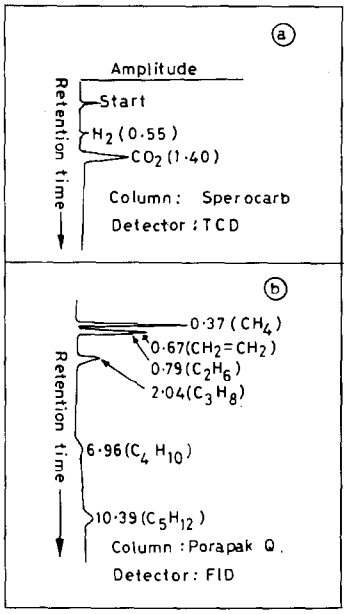

Fig. 5. Gas–liquid chromatograms for gases obtained during the thermal decomposition of $FeC_4H_4O_5 \cdot 2H_2O$ under dynamic nitrogen atmosphere.

microscopy (SEM) showed γ-Fe_2O_2 to be 1–2 μm in length and acicular in shape.

The gaseous products obtained by thermal decomposition of $FeC_4H_4O_5 \cdot 2H_2O$ under a dynamic pure dry nitrogen atmosphere are indicated by the gas chromatograms shown in Fig. 5. These chromatograms show the presence of both types of gases, i.e. polar (H_2, CO_2, etc.) and non-polar (C_2H_4, C_2H_6, etc.). The gases were collected at around 350°C.

The analysis of the various paths of the decomposition of $FeC_4H_4O_5 \cdot 2H_2O$ in various atmospheres showed complete dehydration, as was seen from thermal analysis, conductivity, measurements and the IR spectrum. Transformation of $FeC_4H_4O_5$ to FeO was detected. A separate phase of FeO could not be obtained: it always occurred with $FeC_4H_4O_5$. This mixture of FeO and $FeC_4H_4O_5$ then transformed to Fe_3O_4, which is the final product obtained under dry nitrogen.

$$FeC_4H_4O_5 \cdot 2H_2O \xrightarrow{30\text{–}160^\circ C} FeC_4H_4O_5 + 2H_2O\uparrow \quad (1)$$

$$FeC_4H_4O_5 \xrightarrow{160\text{–}250^\circ C} FeO + C_2H_4\uparrow + 2CO_2\uparrow \quad (2)$$

$$2FeO + FeC_4H_4O_5 \xrightarrow{250\text{–}440^\circ C} Fe_3O_4 + C_2H_4\uparrow + CO_2\uparrow + CO\uparrow \quad (3)$$

The decomposition paths of $FeC_4H_4O_5 \cdot 2H_2O$ in dynamic air, in dynamic

air containing water vapour and in static air were found to be similar, except for the step involving formation of the intermediate γ-Fe_2O_3. In dynamic air containing water vapour a separate step for the formation of pure γ-Fe_2O_3 was detected.

$$FeC_4H_4O_5 \cdot 2H_2O \xrightarrow{30\text{–}175^\circ C} FeC_4H_4O_5 + 2H_2O\uparrow \quad (4)$$

$$FeC_4H_4O_5 \xrightarrow{175\text{–}220^\circ C} FeO + C_2H_4\uparrow + 2CO_2\uparrow \quad (5)$$

$$FeO + 2FeC_4H_4O_5 \xrightarrow{220\text{–}290^\circ C} Fe_3O_4 + 2C_2H_4\uparrow + 2CO_2\uparrow + 2CO\uparrow + [O] \quad (6)$$

$$2Fe_3O_4 + [O] \xrightarrow{290\text{–}350^\circ C} 3\gamma\text{-}Fe_2O_3 \quad (7)$$

$$\gamma\text{-}Fe_2O_3 \xrightarrow{350\text{–}450^\circ C} \alpha\text{-}Fe_2O_3 \quad (8)$$

The gaseous products of the decomposition reaction act as a gas buffer for the solid-state reaction. In fact, it has been suggested that to arbitrarily add a few drops of water to $FeC_2O_4 \cdot 2H_2O$ during decomposition in static air [4] will promote the formation of γ-Fe_2O_3. It should be noted here that γ-Fe_2O_3 obtained in static air is always contaminated with α-Fe_2O_3. This may be due in part to the participation of atmospheric oxygen during the decomposition of Fe_3O_4 because the partial pressure of water may not be sufficient to have the well-separated reaction represented by eqn. (7).

CONCLUSIONS

The present study revealed the following findings on the solid-state dehydration and decomposition of $FeC_4H_4O_5 \cdot 2H_2O$.

(a) Dehydration of $FeC_4H_4O_5 \cdot 2H_2O$ yielding anhydrous $FeC_4H_4O_5$ took place in all three of the atmospheres considered.

(b) The oxidative decomposition behaviour of $FeC_4H_4O_5 \cdot 2H_2O$ was better understood from the study of d.c. electrical conductivity measurements, which showed different regions of conductivity for the intermediates formed, whereas the oxidative decomposition behaviour could not be clearly understood from the thermal curves.

(c) Under the dynamic air atmosphere containing water vapour, pure γ-Fe_2O_3 was formed during the decomposition of $FeC_4H_4O_5 \cdot 2H_2O$.

(d) The gas chromatograms showed that both polar and non-polar gases were obtained during the thermal decomposition.

(e) The scanning electron micrographs, magnetic hysteresis measurements and Mössbauer study showed that the γ-Fe_2O_3 synthesised had all the parameters required for it to behave as an efficient magnetic tape recording material.

ACKNOWLEDGEMENT

The authors are grateful to the Head, Department of Chemistry, University of Poona, Pune 411 007, for his interest and encouragement.

REFERENCES

1 D.J. Craik, Magnetic Oxides, Vol. 2, Wiley–Interscience, New York, 1975.
2 P.D. Pesher and O. Tsyrnorechki, Chem. Abstr., 55 (1961) 9137h.
3 O. Tsyrnorechki and I.V. Arshinar, Chem. Abstr., 55 (1961) 9138b.
4 V. Rao, A.L. Shashimohan and A.B. Biswas, J. Mater. Sci., 9 (1974) 430.
5 K. Seshan, H.R. Anantharam, V. Rao, A.L. Shashimohan, H.V. Keer and D.K. Chakraborty, Bull. Mater. Sci., 3a (1981) 201.
6 K.S. Rane, A.K. Nikumbh and A.J. Mukhedkar, J. Mater. Sci., 16 (1981) 2387.
7 J. Trau, J. Therm. Anal., 6 (1974) 355.
8 A. Venkataraman, V.A. Mukhedkar, M.M. Rahman, A.K. Nikumbh and A.J. Mukhedkar, Thermochim. Acta, 112 (1987) 231.
9 A. Venkataraman, V.A. Mukhedkar, M.M. Rahman, A.K. Nikumbh and A.J. Mukhedkar, Thermochim. Acta, 115 (1987) 215.
10 A. Venkataraman, V.A. Mukhedkar and A.J. Mikhedkar, J. Therm. Anal., 35 (1989) 2115.
11 M.M. Rahman, V.A. Mukhedkar, A. Venkataraman, A.K. Nikumbh, S.B. Kulkarni and A.J. Mukhedkar, Thermochim. Acta, 125 (1988) 173.
12 K.A. Jones, R.J. Acheson, B.R. Wheeler and A.K. Galwey, Trans. Faraday Soc., 64 (1968) 1887.
13 S.D. Likhite, C. Radhakrishnamurthy and P.W. Sahasrabudhe, Rev. Sci. Instrum., 36 (1965) 1558.
14 N.T. McDevitt and W.L. Baun, Spectrochim. Acta, 66 (1964) 255.
15 W.C. Allen, U.S. Steel Fundam. Res. Lab., 1953; ASTM File number 6-615.
16 H.E. Swanson, H.F. McMurdie, M.C. Morris and E.H. Evans, Natl. Bur. Stand. (U.S.), Monogr., 25(5) (1967) 31, 90; ASTM File number 19-629.
17 C.A. Domencali, Phys. Rev., 78 (1950) 458.
18 B.A. Calhoun, Phys. Rev., 94 (1954) 1577.
19 P.A. Miles, W.B. Westphel and V. von Hippel, Rev. Mod. Phys., 29 (1957) 279.
20 R.A. Brown, X-Ray Identification and Crystal Structures of Clay Minerals, 2nd Edn., Mineral Society, London, 1961; ASTM File number 25-1402.
21 W.H. Kelly, V.J. Folen, M. Hass, W.N. Schreiner and G.B. Beard, Phys. Rev., 124 (1961) 80.